Cement and Concrete Composites 74 (2016) 26–38

Contents lists available at ScienceDirect

Cement and Concrete Composites

journal homepage: www.elsevier.com/locate/cemconcomp

Experimental investigation of bond stress distribution and bond strength in unconfined UHPFRC lap splices under direct tension

Fabien Lagier, Bruno Massicotte*, Jean-Philippe Charron

Group of Research in Structural Engineering, Polytechnique Montreal, Montreal, QC, Canada

ARTICLE INFO

Article history:
Received 29 June 2015
Received in revised form
11 July 2016
Accepted 9 August 2016
Available online 31 August 2016

Keywords:
Ultra-high performance fibre concrete (UHPFRC)
Lap splice
Bond stress distribution
Bond splitting strength
Restrained shrinkage
Bar slip

ABSTRACT

Several studies on tension lap splices have shown the improvement of bond strength using Ultra-high performance Fibre Reinforced Concrete (UHPFRC). The bridging effect of fibres on cracks improves the bond splitting strength substantially in comparison to normal concrete. This paper investigates the influence of fibre content on the strength of tension lap splice of reinforcing bars in UHPFRC without additional transverse reinforcement. Different splice lengths and UHPFRC mixes were tested. Internal strain measurements were used to capture the force transfer mechanism and the evolution of longitudinal strain distribution and associated bond stresses. The bond performance is clearly related to the pre- and post-cracking tensile capacity of UHPFRC. At a distance exceeding 2 d_b from bar extremities, bond stress distribution at failure displayed a quasi-constant value regardless of the lap splice length up 10 d_b. This reveals for short lap splices that the bearing action of all ribs along the splice length contributes equally in resisting the applied force. This experimental program provides experimental results for understanding the local force transfer mechanism in UHPFRC lap splice and contribute for further developments on bond in UHPFRC.

1. Introduction

In most practical circumstances, the ultimate bond strength of lap splices is controlled by the member splitting strength due to the bursting forces generated by the ribs of the deformed bars. Tensile strength of concrete is of major importance in such a situation. The development of new generation of concrete such as Ultra-High Performance Fibre Concrete (UHPFRC) offers new solutions for lap splice connections. UHPFRC are mainly characterised by their outstanding ductile tensile properties [1] and extremely low permeability [2]. The role played by splitting cracks in bond failure of lap splice regions emphasizes the importance to control the tensile hoop stresses surrounding lapped bars [3].

In absence of transverse reinforcement, the radial pressure exerted by bar ribs is only balanced by the hoop stresses that develop in the concrete cover surrounding the bars (Fig. 1b). The resisting mechanism to anchor a reinforcing bar depends on the tensile strength and post-cracking energy of concrete. With plain concrete, when hoop stresses reach the tensile strength of concrete, failure occurs by splitting of the concrete cover due to the poor post-cracking energy of unreinforced concrete, causing a sudden drop in the bond resistance. Adding steel fibres in concrete greatly increases the bond performance of deformed reinforcing bars, especially with UHPFRC matrices. Comparison of typical normal strength concrete (NSC) and UHPFRC direct tensile stress-strain properties (Fig. 1a), illustrates that using UHPFRC increases the maximum tensile strength by 2–4 times, provides the concrete a strain-hardening behaviour after first cracking, and enhances considerably the post-cracking behaviour. These outstanding tensile properties generate high and quasi-uniform tensile stresses in the concrete surrounding reinforcing bars (Fig. 1c) that efficiently counterbalance the radial bursting pressure, thereby providing a much better bond performance for the same concrete cover.

Through the improvement of the tensile strength and ductility of UHPFRC, several studies have shown that it is possible to significantly reduce the splice length required to develop the yield strength of reinforcement [4–11] and even reach reinforcing bars ultimate strength [12]. These results allow developing new specifications for connections that could have a particularly strong impact on the design of precast concrete elements for bridges [13] and buildings [9]. Using UHPFRC as a material joint connection

* Corresponding author. Department of Civil, Geological and Mining Engineering, Polytechnique Montreal, P.O. Box 6079, Station Centre-ville, Montreal, H3C 3A7 QC, Canada.
E-mail address: bruno.massicotte@polymtl.ca (B. Massicotte).

http://dx.doi.org/10.1016/j.cemconcomp.2016.08.004
0958-9465/

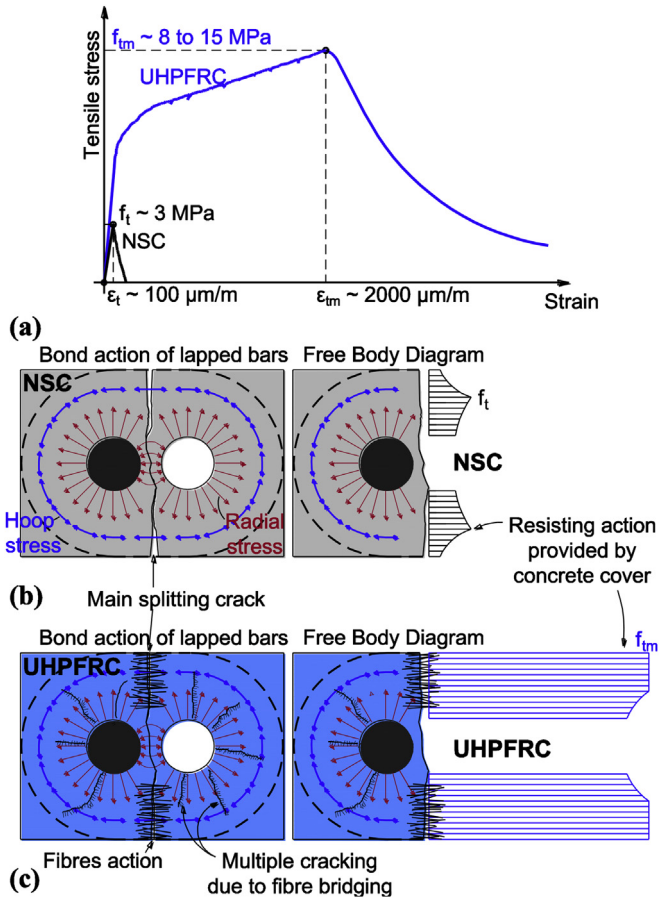

Fig. 1. Concrete cover tensile stresses, (a) typical stress-strain curve, (b) Normal Strength Concrete, (c) Ultra-High Performance Fibre Reinforced Concrete.

simplifies construction details, reduces on site labour work and overall enhances connection durability. Other researchers [14,15] have shown that the most promising retrofit solution for existing bridge piers consists of simply replacing brittle normal concrete cover by a UHPFRC cover all along the surrounding lapped bars at the base of bridge piers. This technique allows eliminating seismic deficiencies such as deficient lap splice reinforcement and stirrup detailing by eliminating the brittle splitting mode of failure, cover spalling and bar buckling [16], thereby allowing bars to reach yielding and finally provide the desire seismic ductility to the structural element. The aforementioned research programs were mainly focused on a global perspective to quantify structural element performance improvement conveyed by UHPFRC lap splice.

The bond stress magnitude reached in these previously mentioned researches varies between 10 and 20 MPa. These values are however significantly lower than those reported on UHPFRC obtained from pull-out tests in which bond stress values range between 35 and 70 MPa [17–20], as discussed by Lagier and Massicotte [11]. Due to the presence of compressive struts between the test support and reinforcing bar ribs, pull-out tests provide bond strength that are not related to the bond mechanism encountered in members in which both reinforcing bars and the surrounding concrete are in tension, such as lap splices. Bond strength obtained from pull-out tests are therefore not applicable for designing lap slices. Despite the knowledge gained on the bond strength of UHPFRC, to the authors' knowledge no experimental program has yet been devoted to examine the local mechanisms in tension lap splice with UHPFRC and the contribution of UHPFRC tensile properties.

For improving the comprehension of bond mechanisms in UHPFRC, an experimental research program was performed at the local level by isolating the lap splice region. For determining the contribution of UHPFRC only, no other reinforcement was provided and the bars were surrounded by a constant thickness concrete cover. The direct tensile lap splice testing procedure adopted provides a relatively simple approach to isolate lap splice zones and enables to reproduce the state of stress obtained in large beam specimens where concrete and steel are jointly subjected to direct tension [21]. This specimen configuration imposes all the tensile force transfer to occur through this isolated element.

The main objective of this research is to determine the contribution of UHPFRC to overcome splitting cracks. To meet the objective, the actual bond stress distribution was obtained by internal strain measurement. This method is the only technique that allows deducing the bond characteristics of steel-concrete interface while maintaining the reinforcing bar surface devoid of any instrumentation system. Through internal strain gauges, a fine detail measurement of steel strain, stress and bond stress were obtained.

In most design codes, semi-empirical statistical approaches have been adopted to determine the bond strength of lap splice. Although these equations are used to reflect the major parameters controlling the strength of a lap splice, their application is restricted to the field of experimental study for which they were derived. Consequently, whenever a new material is introduced, such as UHPFRC, these equations become totally unusable.

The present experimental program aims to provide rigorous and comprehensive bond behaviour that would contribute to developing rational bond strength prediction in UHPFRC from fundamental understanding. Three UHPFRC mixes with different fibre contents and tensile behaviour were selected to reflect a wide spectrum of UHPFRC being available on the market. To some extent, the results of this study can be transposed to other UHPFRC presenting direct tensile behaviour similar to those tested in this research project.

Finally, this study can constitute a useful database for further researches to validate numerical bond simulations with tridimensional detailed bond models with UHPFRC.

2. Experimental program

2.1. Specimen details

For most typical situations of anchorages and splices in reinforced concrete structures, the state of stress in concrete around reinforcement is in tension. The classic pull-out test fails to simulate actual bond condition that occurs in most structural application due to the lateral confining pressure induced along the concrete-reinforcement interface. Using the specimen configuration in which reinforcing bars and concrete are in tension is fundamental to allow a direct identification of the mechanical properties of the bond at the interface. The specimen configuration adopted in this study consists of two pairs of lapped bars cast into a UHPFRC prism that are pulled apart. This test specimen was first adopted by Goto [22] to locally study the crack formation in the concrete surrounding spliced bars, and later used in various studies on bond [23–27]. This specimen configuration corresponds to the local analysis of typical application of UHPFRC in structural members in which the system mechanical strength is mainly governed by the tensile bond performance of lap splice such as in joints between precast elements [13], in column jacketing [16], etc. For isolating the contribution of UHPFRC tensile characteristics on bond

performance, no transverse reinforcement was provided allowing for the total splitting force generated in the lap splice to be resisted only by the tensile stress developed in the UHPFRC cover. All the specimens were deliberately configured to ensure that the reinforcing bars did not reach yielding prior to bond failure to allow gathering data on the ability of different UHPFRC to control and dissipate splitting crack opening due to splitting failure. The specimen dimension and lap splice configuration were designed so that the main splitting crack would occurs within the concrete cover perpendicular to the specimen plane.

The main parameters of the study are the UHPFRC fibre content and the splice length. Deformed 25 mm diameter bars were selected. The specimen cross section was 85 mm thick and 285 mm wide, with a concrete cover of 30 mm for all the specimens, typical of existing structure detail. This corresponds to 1.2 bar diameter (d_b) for the bar size selected in this test series.

Three different UHPFRC were tested with 1, 2 and 4% of fibre volume fractions, V_f. A total of 7 specimens were tested in the experimental program. The notation system used to designate each specimen allows identifying the two main parameters: “Fx-yD”, in which “x” designates the fibre volume fraction in percent and “y” the splice length in term of bar diameter. External and internal reinforcing bars are denoted ER and IR respectively as illustrated in Fig. 2a. Specimen front face (f1, f3) and side face (f2, f4) identifications are reported on Fig. 2b.

3. Materials, mix proportions and curing

The reinforcing bars were made of Grade 400 steel commonly employed in North America and conformed to CSA standard [28] requirements. Geometrical and mechanical properties obtained from three samples tested in agreement with ASTM A370 [29] are summarized in Table 1. The cross sectional area reported in Table 1 represents the average measured value of the reinforcing bar.

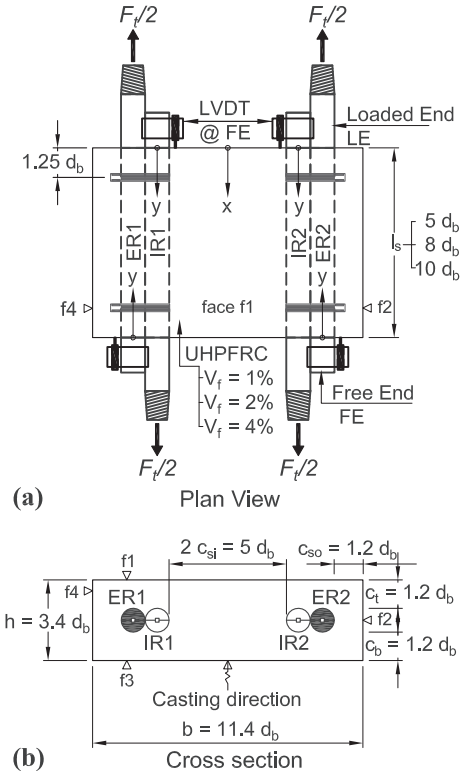

Fig. 2. Details of test specimen.

Table 1
Detailed bar characteristics and properties.

Nominal diameter, d_b (mm)	25
Core diameter, D (mm)	23.4
Average rib depth, h_r (mm)	1.7
Base rib width, a_r (mm)	5.5
Top rib width, b_r (mm)	2.5
Rib spacing, s_r (mm)	17.0
Rib face angle, θ (°)	49
Relative rib area, R_r (-)	0.094
Cross-sectional area, A_b (mm^2)	484
Nominal Young modulus, E_s (GPa)	200
Measured yield strength, f_y (MPa)	460
Measure ultimate strength, f_u (MPa)	659

The three concrete mixes summarized in Table 2 were developed in a previous project [30]. Fibre reinforcement consisted of straight steel fibres (L_f = 10 mm, d_f = 0.2 mm), with a tensile strength of 2600 MPa. Variation in steel fibre volume fraction was compensated by adjusting the sand dosage without changing the W/B ratio. Specimens were cast into wood forms and specific precautions were taken to ensure proper bar alignment. UHPFRC was poured from one location at the centre of the front face f3 to generate a rather random fibre orientation which is similar to actual field conditions. This casting procedure also provides an easily replicable method for all specimens. No vibration was employed because the UHPFRC mixes displayed a self-consolidating mixture allowing an excellent workability. Just after casting, the forms were sealed with a plastic film. During the curing process, specimens were placed on rollers to avoid any external restraint. After demoulding at day one, specimens were subjected to a six-day moist cure after which specimens were stored under laboratory conditions until the testing day.

Material characterisation specimens were submitted to the same curing conditions. Properties were measured at 28 days and on the day of the lap splice specimen testing. Compressive strength, f'_c and Young's modulus, E_c, were determined from 102 × 203 mm cylinders according to ASTM C39 [31] and ASTM C469 [32], respectively. Direct tensile strength was obtained from dog bone specimens with a constant cross section of 100 × 50 mm over a length of 300 mm. Dog bone specimens were produced using several layers over the 50 mm thickness to obtain an appropriate preferential fibre orientation parallel to the applied tensile force. A minimum of three replicate samples for each batch were tested to determine the average compressive strength and the mean behaviour in tension. Young's modulus was obtained from one test only. The main mechanical properties of the UHPFRC for each specimen are reported in Table 3. Fig. 3 presents the idealised average direct tensile curves behaviour of the dog-bone specimens for the seven UHPFRC batches. Experimental response of the pre-peak were simplified by a trilinear curve as proposed by Naaman et al. [33]. Error bars on markers reflect the scatter between test specimens of a same batch. These responses give the optimum tensile strain-hardening behaviour for each mixes with a major preferential orientation and must be considered as the upper limit for each mix.

Results in Fig. 3 illustrate that fibre content affects the stress at the beginning of the strain hardening behaviour, strain hardening modulus (noted as $E_{c,H}$ in Table 3) and the maximum tensile strength (f_{tm}). All fibre dosages exhibited a strain hardening behaviour with a maximum strain before localisation of a macro-crack (ε_{tm}) ranging on average from 10 to 20 times the paste cracking strain (ε_{tp}). The hardening stage must be considered as an equivalent pseudo-plastic phase characterised by very fine

Table 2
Concrete mix design of UHPRFC for different fibre contents.

V_f (%)	Fibres (kg/m^3)	W/B (-)	Cement (kg/m^3)	S. F (kg/m^3)	Sand (kg/m^3)	Superplast. (kg/m^3)	Water (kg/m^3)
1	78	0.20	1012	253	687	30	235
2	156	0.20	1011	253	660	32	234
4	312	0.20	1007	252	604	46	225

Table 3
Splice specimen properties and test results.

Specimen	V_f (%)	l_s (-)	f'_c (MPa)	E_c (GPa)	f_{tm} (MPa)	ε_{tm} (μm/m)	$E_{c,H}$ (GPa)	f_s (MPa)	U (MPa)
F1-5D	1	5	132.3	36.7	5.66	1871	0.508	134	6.6
F1-10D	1	10	138.0	36.2	5.26	1879	0.316	283	7.0
F2-5D	2	5	119.6	37.8	8.27	3130	0.456	164	8.1
F2-10D	2	10	126.3	36.0	8.12	2655	0.412	345	8.5
F4-5D	4	5	115.5	32.0	12.79	2505	1.801	224	11.0
F4-8D	4	8	106.2	36.6	10.48	2013	1.321	350	10.8
F4-10D	4	10	115.1	36.8	13.04	2292	2.032	416	10.3

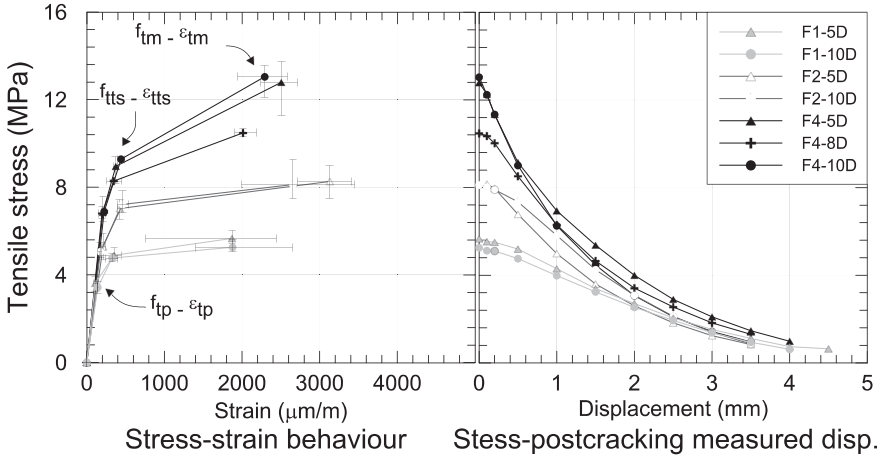

Fig. 3. Idealised tensile properties of UHPFRC batches at 28 days.

microcracks. It is worth mentioning because the values of ε_{tm} are of the same order of magnitude as reinforcement yield strain, that exceptional strain compatibility is expected between steel reinforcement and UHPFRC, leading to much better bond performance than a conventional concrete.

3.1. General instrumentation

A total of eight transverse strain gauges per specimen (with a 50 mm gauge length) were installed on concrete surface at 1.25 d_b from each end on the front faces of specimen (f1 & f3), perpendicularly to the axis of the splice joint (see Fig. 2). This instrumentation was selected to determine the transverse strain magnitude sustained by the UHPFRC cover related to the radial pressure exerted by the ribs on concrete before splitting crack localisation. A total of eight linear potentiometers were also installed above the concrete strain gauge to measure the crack opening during the post-peak behaviour following crack localisation. The loaded end and free end slip of the reinforcing bars were measured by means of LVDTs mounted on a support block attached to the steel reinforcement. The specimen faces were painted in white to detect the onset of cracking on the specimen surface.

3.2. Internal reinforcing bar strain measurement

The experimental procedure was aimed at better understanding the bond stress distribution and the associated bond strength mechanisms in UHPFRC. Detailed evaluation of bond strength and bond performance is complex, as its magnitude is influenced by several factors. The bar stress variation along the bars was achieved with an internal groove in the reinforcing bar which enables maintaining the continuity of contact between the outer surface of reinforcement and concrete. Internal strain measurement was performed because it is an efficient solution to provide realistic bond behaviour without any disruption at the steel-concrete interface [34–41]. This method is the only way to measure the variation of the strain in reinforcement without interfering the desired properties of interface.

From two milled half-bars, longitudinal 4 mm wide and 2 mm deep grooves were milled in each half bar (see Fig. 4) to install 3 mm long strain gauges. Then, the two instrumented half bars were joined together with epoxy glue. The two half bars were intentionally milled with a 100 μm precision to a plane located 0.3 mm above the centroid of the bar to obtain approximately the same cross-sectional area A_s of the original bar. Depending on the specimen length, the gauges were spaced at 11.5 or 23 mm centre-on-centre along the splice length, with the first gauge positioned within the first 10 mm. The gauges were placed alternately on the

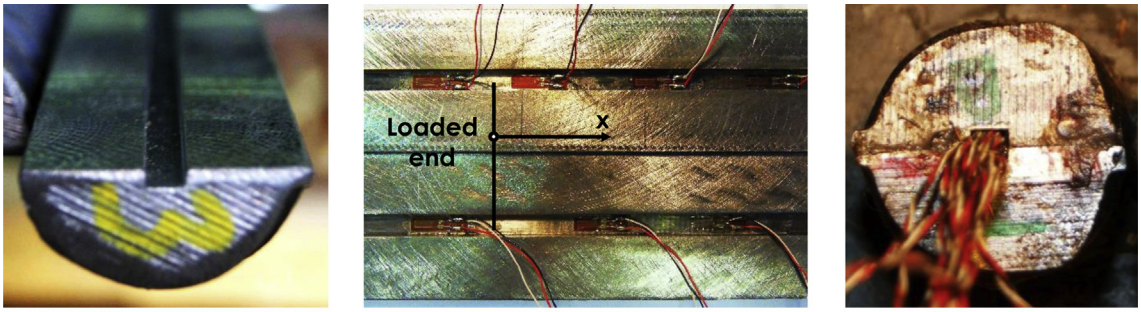

Fig. 4. Internal instrumentation, (a) half bar milled and grooved, (b) typical gauge arrangement of bar ER1, (c) wires at glued bar end.

upper and lower faces of the groove as shown in Fig. 4.

Gauges were also installed on each side of the groove on each bar loaded end outside concrete to determine the applied load. Reinforcing bar strains were recorded from the day of concrete casting up to the tensile test. This allowed measuring bar stress that developed during the curing period, as a direct consequence of UHPFRC volumetric changes due to thermal variation, and autogenous and drying shrinkage, coupled with the beneficial effect of the UHPFRC creep and relaxation under tensile stress at early age considering the elastic modulus variation in time.

3.3. Test set-up and test procedure

Steel bars were fixed to a rigid steel beam system via threaded rods and couplers to ensure that both spliced bars were subjected to the same displacement. The rigid beam system was installed into a 12 MN servo-hydraulic digitally controlled testing frame. Load was applied by displacement control of the two top bars at a constant loading rate of 5 kN/min in the linear stage behaviour. During the test, all the measurements were recorded at the frequency of 1 Hz.

4. Results and discussion

4.1. Mode of failure

All specimens failed by splitting of concrete cover perpendicular to the lap splice plane before reinforcement yielding, following the common approach [42] adopted to predict the maximum splice strength as a function of splice length according to the confinement provided in the lap splice region. Because no transverse reinforcement was provided, the bond strength obtained is directly attributed to the confinement provided by the UHPFRC cover. This allows to properly examine the incident of the different tensile characteristics of UPHFRC such as tensile strength, strain-hardening and fracture energy for controlling bond strength and splitting failure. Results and discussions focus mainly on the lap splice behaviour until reaching the failure load.

The basic force transfer mechanism from one lapped bar to the other through UHPFRC occurs mostly from bearing of the bar ribs on the concrete contact surface [43]. In this test series, inspection of the concrete condition at the interface of deformed bar imprint did not reveal any sign of concrete crushing on the rib front in UHPFRC up to failure [44]. During the first loading step, the concrete cover counterbalances the radial bursting pressure with hoop tensile stresses that remain inferior to the paste tensile strength (f_{tp}) that is significantly higher than for normal strength concrete. Beyond this step, multiple fine microcracks, not visible to the naked eye unless revealed by techniques such as watering concrete surface, form on the concrete surface at the loaded end of the splice in the region where maximum radial pressure is exerted by the ribs. In the tests those fine cracks were only visible on the concrete surfaces around the strain gauges locations (see location Fig. 2) due to the cracking of the transverse strain gauges adhesive, as shown in Fig. 5a. Moreover, although not visible, it is expected that small internal cracks would normally form in the vicinity of the ribs as for normal concrete. However at this stage, the strain hardening characteristics of UHPFRC control the opening of these fine cracks and efficiently counterbalance the radial bursting pressure thereby allowing increasing of the bond strength.

The first visible fine splitting cracks occurred around 75–85% of the ultimate load and were mainly observed at the ends of internal bar (IR) as shown in Fig. 5b. The combination of the radial pressure from the ribs with the effect of lapped bar eccentricity, induces the highest tensile stresses at this location. The splitting crack growth revealed that crack opening was larger on the concrete surface than in the vicinity of the bar (see Fig. 5c and d). The test set-up and specimen configuration provided an excellent observation of the splitting crack initiation directly from the end face of the specimens.

The longitudinal cracks progressed towards the centre along the lap splice through the concrete cover on the front faces (f1, f3) of the specimens. The higher the fibre content, the more efficient the fibre bridging effect contributed to control crack opening and propagation, enabling the lap splices to reach higher bond strength before failure. Fig. 6 illustrates surface concrete cracking patterns at ultimate load (Face f1 only) of each test specimen of 5D and 10D series for the three fibre contents and with the differentiation between fine and macro-cracks.

When the longitudinal cracks began to localise some cracks slightly grew oblique due to the external bars tendency to move outward. After reaching the maximum load, fibres in the matrix started to pull-out, allowing a softening bond failure. The failure was smooth and ductile. After peak load, the bond strength decreased gradually due to the splitting crack propagation. This softening behaviour can be attributed to fibre bridging effect. Detailed study on the splitting crack opening behaviour on similar specimen with UHPFRC can be found in Lagier et al. [11]. All specimens show an outstanding damage tolerance during post-cracking propagation without any spalling of concrete (see Fig. 5d).

4.2. Bond strength

Table 3 summarises the results of the tested specimens at ultimate load. Maximum bar stress and average bond strength values are reported. The average bond-stress u at failure is determined by

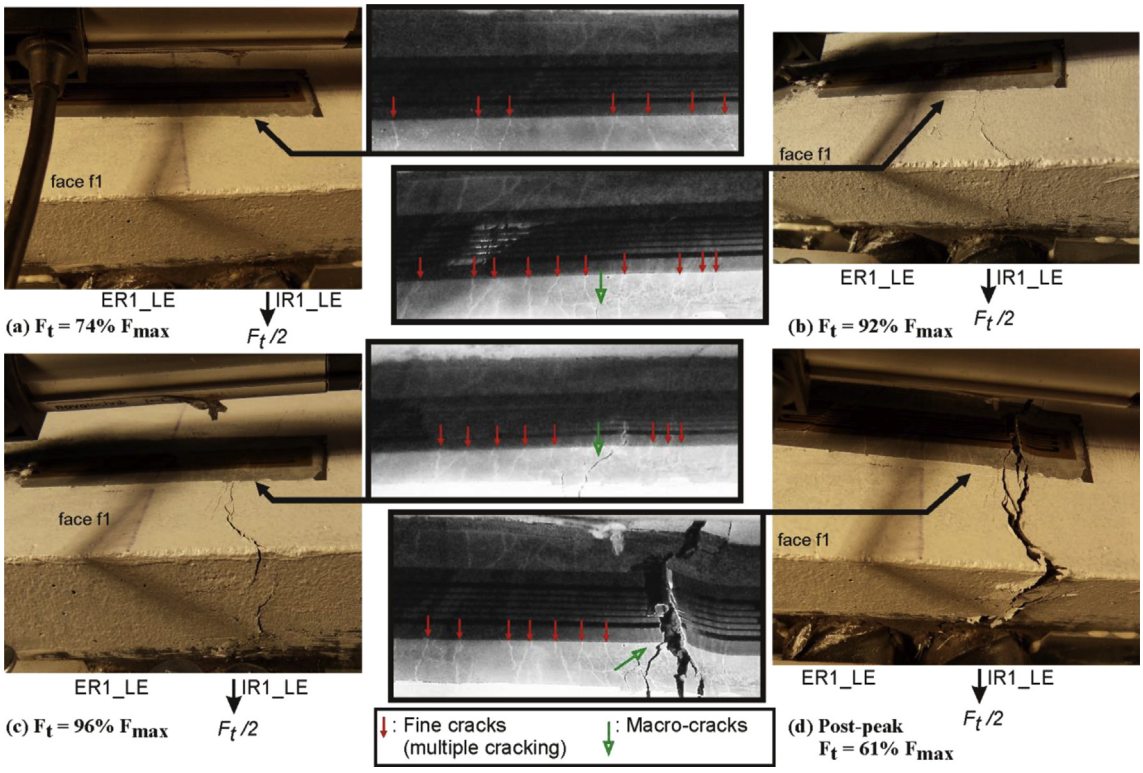

Fig. 5. Fine crack and macro-crack evolution at loaded end of bar IR1, face f1, specimen F4-10D.

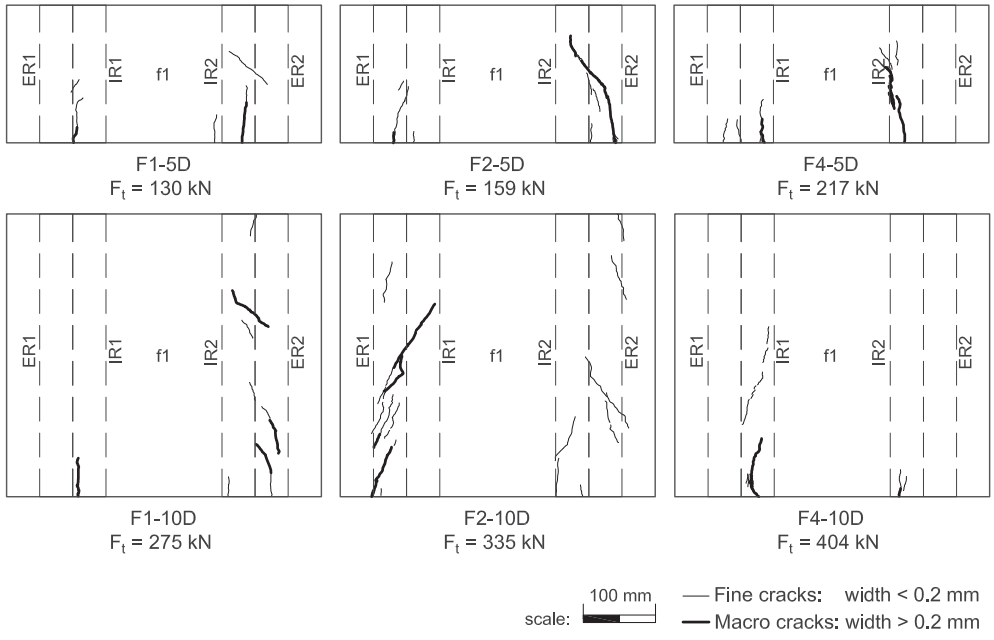

Fig. 6. Surface concrete cracking patterns (Face f1) in test series 5D and 10D at ultimate load.

assuming that bond is constant over the splice length, according to:

$$u = \frac{A_b f_s}{\pi d_b l_s} \quad (1)$$

where f_s is the bar stress and l_s the splice length.

From this experimental program all specimen with 4% fibre content showed a very similar average bond stress slightly superior to 10 MPa. This indicates that there is no drastic loss of effectiveness of the bond strength by doubling the splice length within the parameter range considered. Increasing the amount of fibres has a positive effect on the bond strength. As expected, using higher fibre dosage increases UHPFRC tensile properties and allows developing more important hoop stress in the surrounding concrete to counteract the outward pressure from ribs. For a given splice length of 10

d_b, an increase of the volume fraction from 1% to 2% and 4% led to a considerable increase of the ultimate bond stress of 22% and 47% respectively. The test results indicate that UHPFRC with 4% fibre content steel stress over 400 MPa was reached, close to yielding. Then, the splice length required to develop the bar yielding can be considerably reduced compare to current design requirement. In a previous study carried out by the authors [11], a 4% fibre dosage was found to be sufficient to achieve reinforcement yielding for a splice length of only 12 d_b. However reaching yielding is not the sole criteria and providing a ductile lap splice failure mode would necessarily lead to a safer and more efficient design, which was entirely achieved using high fibre content UHPFRC. More detailed information about post-cracking behaviour on similar specimens can be found in Lagier et al. [11].

4.3. Longitudinal steel strain and equivalent bond stress distribution

Experimental results presented in Table 3 can be better understood and interpreted from the bond stress distribution. Fig. 7 shows an example of the strain distributions in the reinforcing bars (ER1, IR1, ER2, IR2) and the associated bond stresses along the specimen length for specimen F4-10D. The various loading levels are identified by different sets of markers corresponding to the experimental acquisition of strain gauges inside the reinforcing bar. From these experimental data point, a fourth degree polynomial curve fitting was applied (see Fig. 7a and c) to adequately describe the steel strain distribution. The second ordinate in Fig. 7a and c shows the equivalent tensile stress in the bar. The loading level at 0% reflects the initial state of stress that corresponds to the end of the curing period due to the restrained shrinkage effect.

The close spacing of gauges (11.5 or 23 mm) inside the bars allowed capturing a very detailed strain distributions in the bar and provides an accurate determination of the associated bond stress distribution and its evolution under loading. Based on the equilibrium of forces, the bond stress between strain gauges can be calculated as follows:

$$\tau_j = \frac{E_s A_s}{\pi d_b} \frac{\varepsilon_{s,i+1} - \varepsilon_{s,i}}{y_{i+1} - y_i} \quad (2)$$

The bond stress calculation was performed according to each bar longitudinal axis with the axis origin located at the bar free end (Fig. 2).

This relationship indicates that the bond stress distribution is directly proportional to the gradient of deformation between two strain measurement points. Bond stress is consequently very sensitive to a small variation of strain. Thus, the bond stress was determined directly as the derivative of the smoothed curve which results in a third degree bond curve, as presented in Fig. 7b and d.

Unlike tests conducted on normal concrete [38] and high strength concrete [26], there are very small discrepancies and irregularities between consecutive experimental measurements in UHPFRC specimens. No abrupt rise in the reinforcement strain related to the onset of transverse crack appears up to failure due to the pseudo plastic phase with a large strain capacity offered by UHPFRC (>2000 μm/m). In this context, the use of internal strain measurement is particularly relevant and its interpretation is greatly facilitated. Although the data smoothing method used has certain limitations close to the ends of the splice lengths according to the selected degree of the polynomial curve and due to the stress distribution irregularity, the use of a third degree bond relationship reproduces adequately the bond stress distribution along lapped bars and bond stress evolution during the loading stages.

In all specimens the force difference at ultimate load between the two pairs of lapped bars was less than 10%, except for the specimen F2-5D in which a force difference of 12% was measured. As expected, steel strains are larger at the loaded end of the bars and reduce progressively towards the unloaded end, where bars are at zero strain. For all the specimens, the bars remained elastic because all tests were designed to have a splitting failure in the UHPFRC before yielding of reinforcing bars.

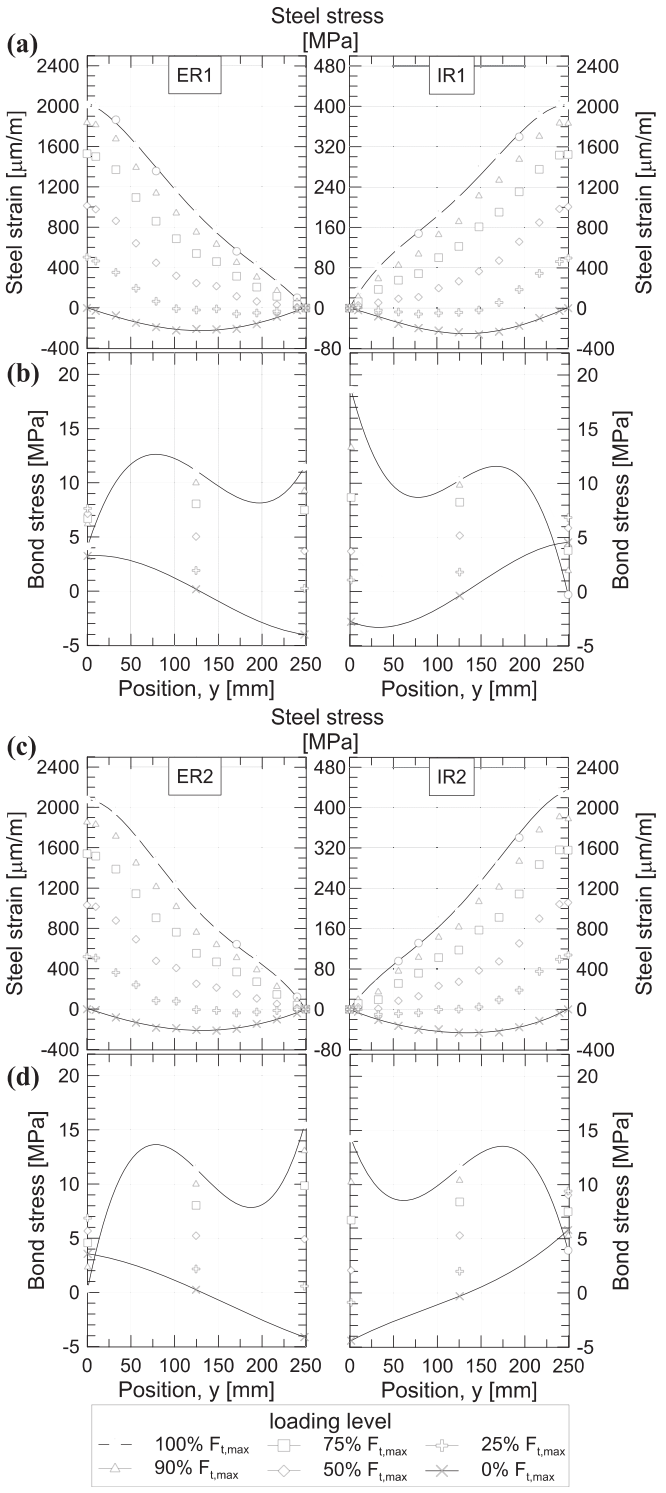

Fig. 7. Specimen F4-10D internal measurement at 0%, 25%, 50%, 75%, 90% and 100% $F_{t,max}$; (a) steel strain, (b) bond stress, (c) steel strain, (d) bond stress.

In the early loading stages, the initial stress condition due to the restrained shrinkage had a significant influence on the steel stress transfer distribution. At a loading level $F_t = 25\%$, the active bond stress was spread over approximately half of the available splice length. Fig. 7b and d shows that higher bond stresses developed close to the loaded end of the bars at the beginning of the tests while low bond stresses were mobilised in the specimen middle zone. As loading increased, the bond stress distribution spread over the entire splice length.

A steep steel strain gradient developed at the spliced bar free end over a short distance, a feature specific to lap splices [3]. It illustrates that force transfer takes place over a short distance at the lap ends. It is characterised by a peak in bond stress distribution presents at the free end. As the load increases, the maximum local bond stress increases together with the average value. For high applied load (>50% F_t), the steel strain amplitude close to the loaded end progressively flattens due to the progressive degradation of the interface. Consequently the maximum bond stress that occurs near the loaded end in the early stages moves inward as the applied load increases whereas bond stress decrease to zero at the loaded end due to the splitting cracks, which initiated at ≈80% F_t mostly at the internal reinforcing bar (IR) where the bond stress is maximum. Then, up to failure, the splitting cracks propagated along the spliced bar and the peak of bond stress at free end increase continuously to become the maximum local bond stress at ultimate load.

The influence of restrained shrinkage, splice length and fibre contribution can be analysed and compared at the local scale through the difference in steel stress and the bond stress distribution. Fig. 7 shows that the strain distribution and its evolution during loading are comparable between the two pairs of lapped bars. Therefore, only one side of the lap splice specimen will be selected and presented in the following sections. The selected side is the one for which the splitting crack was opened the most at ultimate load, namely bar side ER1/IR1 for specimens F4-10D, F4-8D, F2-10D, F1-10D and bar side ER2/IR2 for specimens F4-5D, F2-5D, F1-5D.

4.4. Influence of restrained shrinkage

Due to a low water/binder ratio and high cement content, UHPFRC is particularly sensitive to autogenous shrinkage during the hydration process [45]. Concrete shrinkage in reinforced concrete members is always restrained by the reinforcing bars, which generates tensile stresses in the surrounding concrete. Early age cracks may arise when the tensile stresses in the concrete due to the restrained shrinkage become higher than the tensile strength of concrete at that age.

Fig. 8 shows the evolution of the total strain measurement in the reinforcing bars inside the specimen during the curing period for gauges located at the centre of the specimen for series 10D, and 11.5 mm away from the centre for the test series 5D. The total strain represents the average strain measurement of the 4 bars at the same location. A gross reinforcement ratio of 8% is present in the specimens. The strain and associated compressive stresses developed in the bars are the direct consequences of UHPFRC shrinkage coupled with its viscous response under tensile stress at early age.

On Fig. 8, time t begins when concrete is placed in the moulds. The first effect of the restrained shrinkage by the bars begins the first day of hydration between 12 h and 18 h depending on the specimen. During the curing period, only autogenous and thermal shrinkage are present. At the end of the wet curing period (day 7), the contribution of drying shrinkage adds up, visible on Fig. 8 by a clear change in the average steel strain gradient. The difference of kinetics evolution of the steel strain over the curing period for a given splice length is explained by the difference in temperature in the laboratory during the maturation period. Indeed, a temperature difference in the laboratory of 10 °C between specimens cast during the summer (F1-5D and F1-10D) and winter periods (F4-5D and F4-10D) was noted.

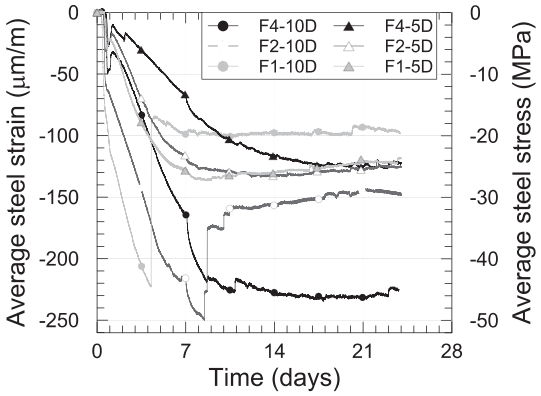

Fig. 8. Steel strain and stress evolutions at mid length for series 5D and 10D specimens.

First, the longer the splice length, the more important the steel strains, and consequently the higher the cracking potential. After 24 days, for shorter specimens (series 5D), the influence of the fibre content on the total restrained shrinkage is minor. For longer specimens (series 10D), a fine transverse crack appeared near the centre during the curing period. In this case, specimens with higher fibre content exhibited a lower reduction of the steel strain and finer cracks, which opening was better controlled by the higher number of fibres crossing this early fine transverse crack.

In term of concrete stress, the average shrinkage stress in UHPFRC, σ_c, can be calculated based on the equilibrium of forces between reinforcing bar and the net concrete area. At 24 days, a maximum tensile stress of 4.0 MPa was reached for specimen 10D-F4.

4.5. Effect of splice length

Fig. 9a shows the steel stress distribution of internal bars designated IR for specimens with different splice lengths and fibre dosage of 4%. The steel stress distribution is plotted at the end of curing just before loading and for a given steel stress of $f_s = 160$ MPa in the reinforcing bars, corresponding to loading level $F_t = 155$ kN before splitting cracks were initiated.

At this loading stage the splice length does not particularly affect the rib mobilisation to develop a given stress. Thus, for all the different splice length, the distance required to develop any given stress at this stage was relatively similar. Fig. 9b shows the distribution of the associated bond stress along the splice length. With a decrease of splice length, the peak of local bond stress increases in the specimen. This observation is also valid for the peak of bond stress visible at the free end.

Fig. 9c shows the steel stress and strain distribution in the same bar when the ultimate load of the specimen was reached. First of all, as expected, the longer splice was able to carry a greater load, with the ability to mobilise all ribs within the lap length. As the strain increased in the reinforcing bar, the formation of splitting cracks in the vicinity of the loaded ends affects appreciably the steel stress distribution. At each bar loaded end the strain amplitude eventually flattened, more or less pronounced according to the splitting crack growth and its opening along the bar. At the other end, however, a steep steel strain gradient is noticeable over a short length.

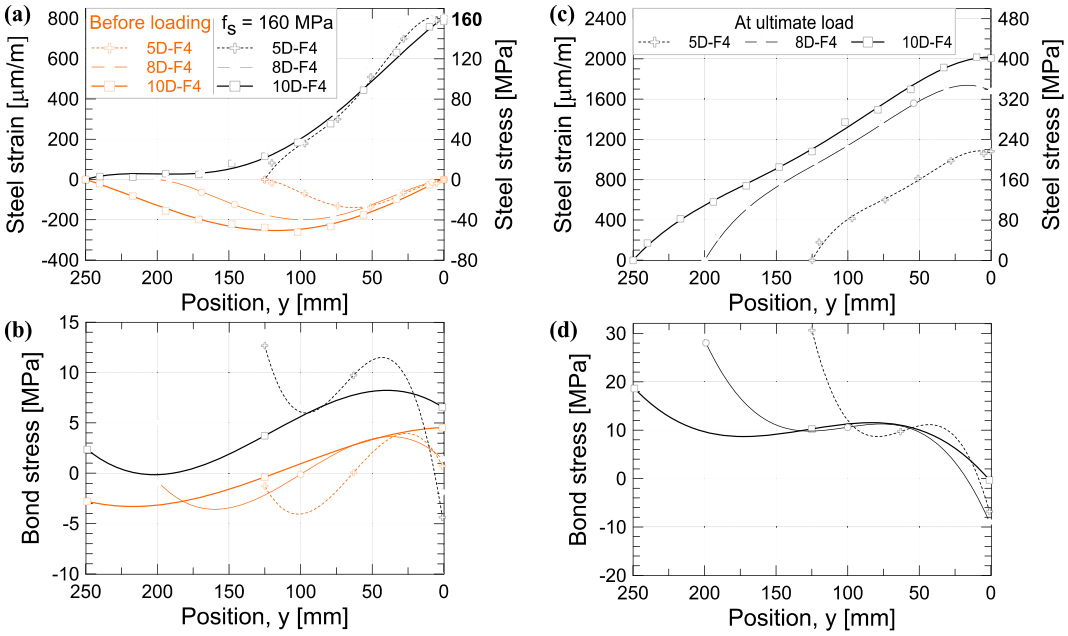

Fig. 9. Steel strain and stress, and equivalent bond stress distribution along the spliced bars IR; (a)&(b) before loading and $f_s = 160$ MPa, (c)&(d) at ultimate load with UHPFRC 4%.

At ultimate load, the peak value of the bond stress at free end varies according to the state of bond degradation in front of the ribs from the loaded end, as seen in Fig. 9d. The steel strain distribution in UHPFRC displayed a quasi-linear increase of strain associated to a more or less uniform bond stress, except for over a distance varying from 1 to 2 d_b at each extremity. This directly implies that all ribs along the splice length evenly participated in resisting the total applied load. It is interesting to note that the strain gradient in this portion of the splice length is relatively similar for the 3 specimen lengths. As shown on Fig. 9d, bond stress values vary within a narrow range, between 10.5 and 12.5 MPa. Hence, unlike high strength concrete, doubling the splice length from 5 d_b to 10 d_b in the UHPFRC led to an increase of bond strength due to the contribution of each bar rib along the splice. This is attributed to the action of fibres that efficiently bridged the longitudinal cracks and provided a considerable confinement improvement.

4.6. *Effect of fibres*

The steel stress distribution from 1 bar to the other and the associated bond stress distribution of the lap splice series 5D and 10D are plotted in Fig. 10 and Fig. 11 respectively where the three volume fraction of fibres are compared. For series 5D, Fig. 10 shows experimental data before loading, for a steel stress $f_s = 100$ MPa in the reinforcing bars and at ultimate load. Fig. 11 shows experimental data before loading, for a steel stress $f_s = 230$ MPa in the reinforcing bars and at ultimate load for series 10D. The 100 MPa and 230 MPa values were selected to have a similar steel stress ratio with respect to the ultimate load of test series 5D and 10D.

For series 5D, the tensile stress generated in the concrete during curing due the restrained shrinkage is identical for the three fibre volume fractions (Fig. 10a). For $f_s = 100$ MPa, no splitting crack was visible on the concrete surface. At this load level, it may be already noted that from the loaded end of the reinforcing bar, a longer distance is required for IR bar to develop 50% of f_s along the splice length. This indicates a possible decrease in bond performance at the interface of the internal bars (IR), although no visible splitting crack on the surface were observed.

For a given position along the splice, the stress in the bar is lower with the larger amount of fibres. Thus, the offset between the stress distributions of the internal bar according to the percentage of fibres illustrates the increased performance of the steel-UHPFRC interface with the increase of fibre content used. This observation was also noted in the case of the 10D series (see Fig. 11a). At the end of curing for specimens 10D-F1 and 10D-F2 (Fig. 11a), the measured steel stress distribution was disturbed by the occurrence of transverse shrinkage cracks. For specimens for which transverse shrinkage cracking occurred during the curing period, the 0% polynomial curve was not plotted. In this case, the bond stress points in Fig. 11b were calculated directly from the experimental data. However, the fine transverse cracks that formed during curing have a limited influence on the steel strain distribution at higher loading. None of these transverse cracks have had an impact on the mechanical response and cracking to rupture.

In terms of bond stress distribution at low load level (Figs. 10b and 11b), the observations are similar between the two series. The maximum local bond stress is reached for specimens with the highest fibre content. Indeed, for specimens 5D and 10D with 4% fibre content, the bond strength is mainly mobilised in the first half of the specimen while at free end low bond stresses were developed. In general, the decrease in the amount of fibres implies a greater degradation of the bond near the loaded end. Consequently the peak bond stress shifts inward the specimen. For specimens with a splice length of 10 d_b, this corresponds to a relatively uniform bond stress distribution after a distance of 2 d_b from the loaded end.

At the ultimate load of the 5D series (see Fig. 10c and d), the steel stress distribution presents a clear uniform stress distribution at the loaded end that can be directly related to the progression of the splitting crack. On the opposite side, from the free end of the bar IR, a very steep strain gradient forms over a short splice length. This confirms a link between the bond stress degradation at the vicinity of loaded end and the steep strain gradient in the reinforcing bar noticeable at the free end. Nevertheless, as described in the mode of failure section, the initiation of longitudinal cracks did not result in failure of the specimens due to the performance of UHPFRC. Cover

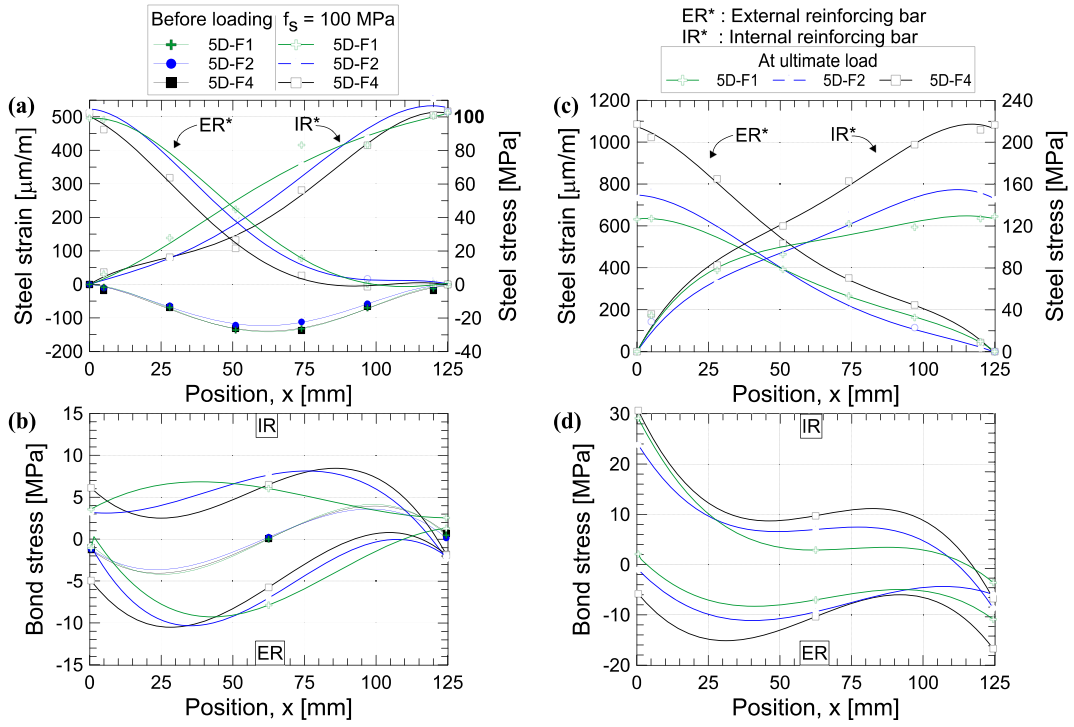

Fig. 10. Steel strain and stress, and equivalent bond stress distribution along the spliced bars; (a)&(b) before loading and f_s = 100 MPa, (c)&(d) at ultimate load - Series 5D.

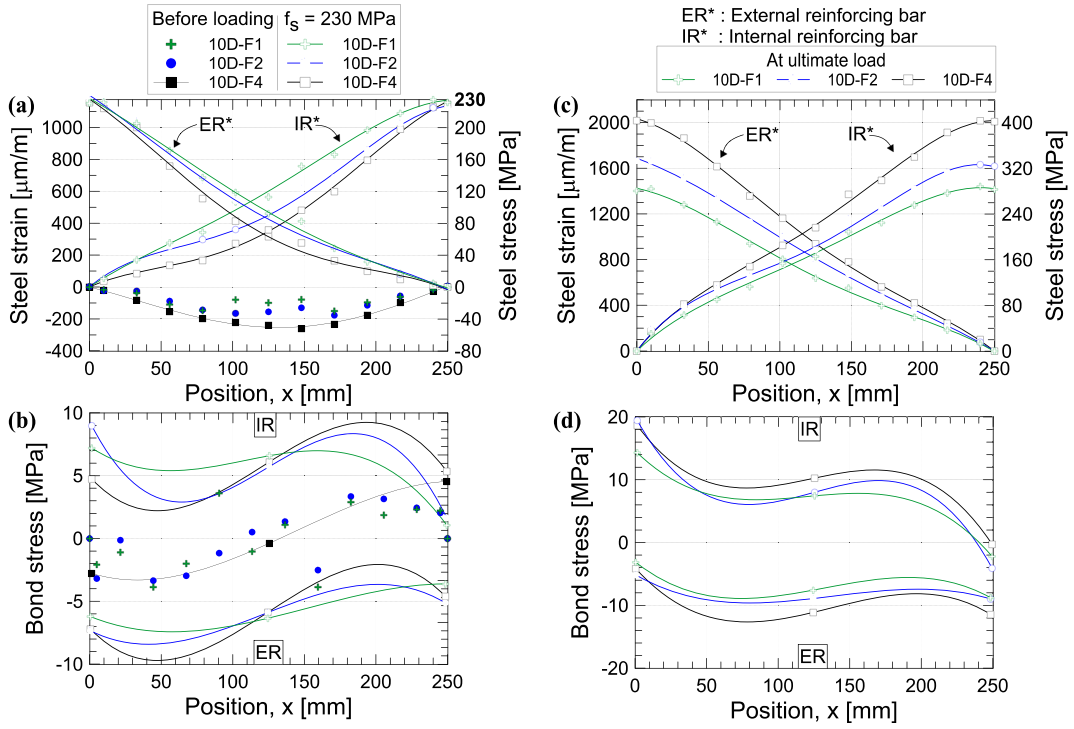

Fig. 11. Steel strain and stress, and equivalent bond stress distribution along the spliced bars; (a)&(b) before loading and f_s = 230 MPa, (c)&(d) at ultimate load - Series 10D.

splitting occurred at load level around 75%–85% of the ultimate load for all specimens. The splitting crack resulted in a progressive decrease of the local bond stress at the loaded end. However, the strain-hardening properties of UHPFRC surrounding the spliced bars ensured an efficient splitting crack control and propagation that allowed bond stress to be developed in the fracture process zone. Moreover, for all specimens (Fig. 6), the main splitting crack progressed more than half the splice length before observing a decrease of the total bond strength.

In Fig. 10c and d and Fig. 11c and d bond degradation is visible close to the end of the internal bar where the main splitting crack propagated. This is evidenced through the plateau shown in the

figures presenting the steel stress distribution near the end of bar IR (Figs. 10c and 11d), more or less pronounced depending on the opening of the splitting crack. Consequently, the equivalent bond stress distribution for bar IR at this location shows a sharp decrease to a zero bond stress (Figs. 10d and 11d). This bond stress degradation increases for lower fibre volumes. At a distance of 1 db from each bar loaded end, the decrease of bond stress between the bar IR and bar ER varies from 58% to 29% with volume fraction from 1% to 4% respectively. Moreover, it is interesting to note that when a splitting crack forms at the loaded end of a bar, the loss of bond does not necessarily affect tensile force in the adjacent spliced bar because the fibre action still ensures enough cohesion between the two overlapping bars. This phenomenon is attributed to the ductile behaviour of UHPFRC. Hence, in Fig. 10c, despite the presence of a uniform strain at the loaded end of bar IR2 in series 5D, the performance of UHPFRC allowed mobilising the bar ER2 at the same location, where a gradual increase of strain was recorded.

At ultimate load, for short specimens (see Fig. 10d), the bond stress distribution is relatively uniform over the splice length for external bars, contrary to internal bars where the stress variation is larger. It is clearly visible that the steel stress distribution of internal reinforcing bar is not linear along the lap splice.

4.7. Steel stress ratio versus transverse concrete strain

In Fig. 12, the bar stress ratio (f_s/f_y) for the internal reinforcing bars (IR) are plotted with respect to the transverse strain measured on opposite face (f1 or f3) at 1.25 d_b from the loaded end of the lap splice specimen (Fig. 2). The maximum stress $f_{s,max}$ represents the average stress of the four reinforcing bars. Curves are shown up to peak load. Results of this analysis showed that the overall transverse strain evolution with the increase in steel stress ratio in the bar can be characterised mainly by two stages. The first stage, in which the steel stress ratio increases significantly up to a certain deformation ($\varepsilon_{tp} \approx 200$ μm/m), corresponds to the strain at the limit of elasticity measured in direct tensile tests on UHPFRC. Beyond this point, gain in strength continued until it reached the maximum steel stress that can be developed according to the fibre dosage with large inelastic strain in the UHPFRC. In this second stage, for an equivalent transverse strain increment, higher fibre content allows increasing the stress level developed by reinforcing bars. This observation shows that the transverse strain evolution during the bar loading is closely related to the tensile behaviour of UHPFRC under direct tension. Fig. 12 emphasizes the participation of the UHPFRC cover in tension around spliced bars to counterbalance the radial bursting pressure generated by the action of ribs. Similar results were obtained in lap splices with 35 mm bar diameter [11]. For each test, despite the initiation of macro cracks at the end of some face, which provoked the loss of strain gauge reading and are marked by a cross symbol in Fig. 12, the UHPFRC cover surrounding lap splice bars continues to contribute to an increase in the maximum bond strength. As an example for specimen 25-F2-10D, at a bar stress ratio above 0.63, two splitting macro-cracks were initiated and progressed in bar IR1 face f1, and in bar IR2 face f3. Though, transverse strains recorded on the opposite face of cracks show that after this stress is reached, UHPFRC continues to resist to the bursting force and ensure an increase of steel stress in internal bars.

4.8. Bond-slip response of spliced bars

Bond stress slip curves are plotted in Fig. 13 in which the free end slip s is the average value of the two internal reinforcing bars, IR1 and IR2. The bond stress-slip curve from all tests series follows

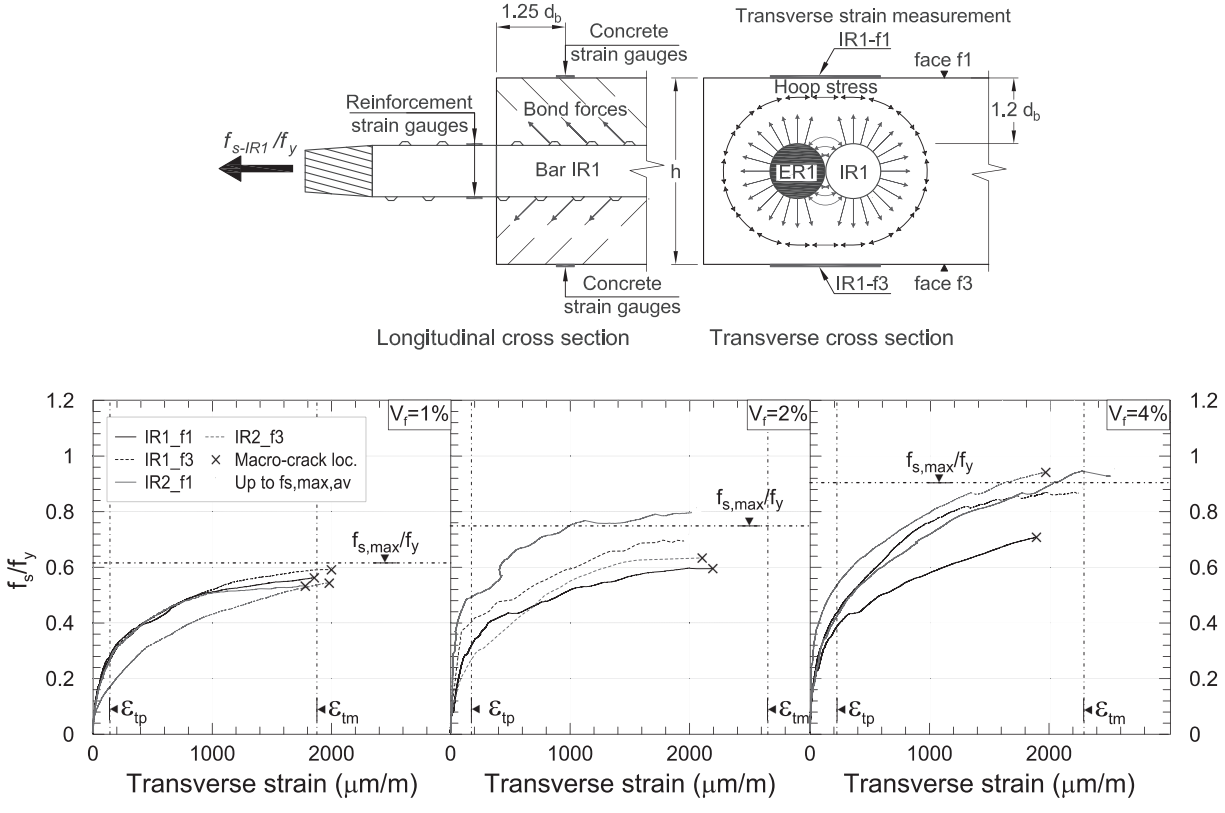

Fig. 12. Steel stress ratio in internal reinforcing bars vs transverse strain at 1.25 d_b from the splice end.

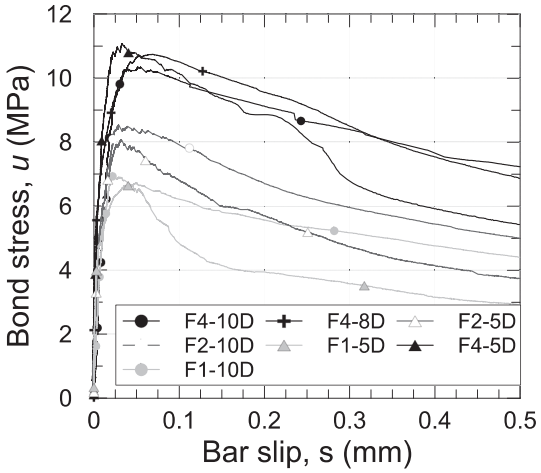

Fig. 13. Bond stress-slip response.

the same basic shape. All the series show a nearly identical initial stiffness that is practically independent of the fibre content: first a very steep rise in bond strength with minor end slip, until splitting crack initiates around 80% of the ultimate bond strength, and then a splitting crack propagation phase in which the bond stress kept increasing as bar slip increased until a peak bond strength was reached. Free end slip did not exceed 0.05 mm at peak load for all 5D and 10D series. Beyond this point, the bond strength capacity decreased gradually with a further progression of slip.

The homogeneity of UHPFRC matrix provided by small aggregate size, high compactness and high binder content, gives a considerable improvement of the bond performance at the bar interface especially, in front of each rib. After failure, bond-slip behaviour is typically marked by a net increase of loaded end slip with the progression of splitting cracks. At this stage, contrary to normal concrete, a gradual bond stress reduction occurred, controlled by fibre action.

Cairns and Plizzari [46] proposed a slip criteria at the free end that should not be exceeded to ensure adequate structural performance of a lap splices. According to his recommendation, slip at the unloaded end should be less than 0.1 mm for a developed steel strain of $\varepsilon_s \approx 0.002$ at the loaded end of nominally confined lap splices. The maximum strain in specimen F4-10D exceeded that value while the corresponding free end slip value was of 0.045 mm, which is more than two times smaller the proposed criteria. Hence this study shows that very short lap splice in UHPFRC with 4% of fibre volume fraction can easily fulfil the proposed requirement.

5. Conclusion

In this study, direct tension lap splice tests were carried out to assess the bond strength and bond stress distribution in specimens embedded in UHPFRC. Specimens were designed to fail by bond splitting before reaching the yield strength of the reinforcing bars. The investigation objectives were to determine the contribution of UHPFRC with different fibre contents and variable lap splice length on the performance of reinforced concrete member lap splices, and to evaluate the bond splitting behaviour with the only confinement provided by UHPFRC cover. Test results indicated that confinement with UHPFRC is an extremely promising solution with high potential for the enhancement of bond performance in splice regions. From the results and analysis of the seven tests with three different splice lengths and fibre contents, the following conclusions can be drawn.

1 Internal strain measurement, which was implemented in this study, was an extremely effective way of measuring longitudinal strain distribution along lap splice. Through this method, it has been possible to obtain refined information without disturbing the interface area between steel and concrete. It has proven that it was an effective procedure to obtain bond stress distribution in UHPFRC. Since no transverse cracks developed through the section up to failure, the bond stress was not disturbed by other cracks than longitudinal splitting crack.
2 Steel stress distribution can be characterised mainly by three sections. At free end, a steep gradient is being developed over a short distance, characteristics of force transfer between spliced bars. On the opposite, at loaded end as the load increased to splitting failure, steel stress amplitude reaches a maximum value and the distribution becomes progressively flattened due to progressive degradation of the interface. Between the 2 bar extremities, steel stress distribution displayed a quasi linear increase of stress regardless of the lap splice length used.
3 Bond stress distributions are associated to steel stress variation and consequently characterised by three stages, two local peaks at free and loaded ends, and a quasi-constant bond stress distribution between these two regions. Before splitting crack is visible (<80% F_t), peak bond stress was always noted close to the loaded end. As the load increase, first peak bond stress move inwardly, and the peak bond stress at loaded end reached a maximum value, which magnitude is related to the splitting crack propagation from loaded end.
4 For a given position inside the lap splice, the steel stress developed in the bar is lower with a greater fibre contents used in the UHPFRC.
5 The evolution of transverse strain measured on the concrete surface close to the end of splices with respect to the evolution of the bar force of lap splice specimens emphasise the contribution of UHPFC tensile properties in its strain hardening stage to counterbalance the radial bursting pressure. Maximum splice strength capacity is clearly related to the inelastic capacity and strain hardening performance of UHPFRC. Fibres play a key role in increasing the maximum strength of lap splice specimen.

Moreover, in term of global performance, average bond stress superior to 10 MPa was obtained for all specimens with 4% of fibre dosages. Specimen F4-10D was able to develop a steel stress over 400 MPa close to the bar yielding with free end slip of 0.045 mm for a developed steel strain of $\varepsilon_s \approx 0.2\%$, that is less than two times the slip limit criterion introduced by Cairns and Plizzari [46]. Theses observation shows the potential of reduction splice length required to reach design criteria.

In the case of a structural members sensitive to shrinkage crack formation at early age due to high reinforcement ratio, large contact surface with old concrete, etc., higher amounts of fibres control efficiently the progression of the transverse crack. In this test series 4% by volume was sufficient whereas 2% was not. Brühwiler and Denarié [47] recommended a minimum of 3% for thin repairs to avoid restrained shrinkage cracks.

As stated by CEB-FIP 2000, “For the time being, standard bond tests must be considered of limited value, and any new reinforcing materials need to be tested for bond performance in structural elements under conditions representative of practice”. The only ultimate bond strength cannot be stated to provide enough information on the bond performance. This study has attempted to explore in a more comprehensive way the bond performance of lap splice in UHPFRC. The specimen configuration and test arrangement used in this study allowed a reasonable representation of bond condition in real situation. Both reinforcing bars and concrete are subjected to tension, the most common situation in structural

applications. This experimental program constitutes a unique and useful database reference for FE modelling of bond with UHPFRC.

Acknowledgements

The financial support was provided by Quebec Ministry of Transportation (Project R685.1), and the Natural Science and Engineering Research Council of Canada (NSERC), through the Canadian Seismic Research Network (350698-97) and the Discovery Grant (105623-01) programs. The research was carried out in Polytechnique Montreal *Hydro-Québec* Structures Laboratory. Some materials were graciously provided by Bekaert and Euclid. The authors would like to express their gratitude to the laboratory professional and technical staff for their valuable assistance during the preparation and testing of the specimens.

References

[1] K. Habel, J.-P. Charron, S. Braike, D. Hooton, P. Gauvreau, B. Massicotte, Ultra-high performance fibre reinforced concrete mix design in Central Canada, Can. J. Civ. Eng. 35 (2008) 217–224.
[2] J.-P. Charron, E. Denarié, E. Brühwiler, Permeability of ultra high performance fiber reinforced concretes (UHPFRC) under high stresses, Mater. Struct. 40 (3) (2007) 269–277.
[3] R. Tepfers, A Theory of Bond Applied to Overlapped Tensile Reinforcement Splices for Deformed Bars, Chalmers University of Technology, Goteborg, Sweden, 1973.
[4] F. Lagier, B. Massicotte, J.-P. Charron, Bond splitting of lap splice embedded in ultra high fibre reinforced concrete under direct tension, in: J.W. Cairns, G. Metelli, G.A. Plizzari (Eds.), Proceeding of the 4th Conference on Bond in Concrete 2012: Bond, Anchorage, Detailing. Brescia, Italy, 2012, pp. 351–358.
[5] L.F. Maya, C. Zanuy, L. Albajar, C. Lopez, J. Portabella, Experimental assessment of connections for precast concrete frames using ultra high performance fibre reinforced concrete, Constr. Build. Mater. 48 (2013) 173–186.
[6] A.K. Cheung, C.K. Leung, Effective joining of pre-cast concrete slabs with self-compacting HSFRCC, J. Adv. Concr. Technol. 9 (1) (2011) 41–49.
[7] B. Graybeal, Behavior of Ultra-High Performance Concrete connections between precast bridge deck elements, in: PCA (Ed.), Proceeding of 2010 Concrete Bridge Conference: Achieving Safe, Smart & Sustainable Bridges. Phoenix, USA, 2010, pp. 1–13.
[8] P. Harryson, High performance joints for concrete bridge applications, Struct. Eng. Int. 13 (1) (2003) 69–75.
[9] B. Aarup, B.C. Jensen, Bond properties of high-strength fiber reinforced concrete, ACI J. Sp. 180 (1998) 459–472.
[10] J. Yuan, B. Graybeal, Bond Behavior of Reinforcing Steel in Ultra-high Performance Concrete, FHWA-HRT-14-090: US, Department of Transportation, Federal Highway Administration, 2014, p. 78.
[11] F. Lagier, B. Massicotte, J.-P. Charron, Bond strength of tension lap splice specimens in UHPFRC, Constr. Build. Mater. 93 (2015) 84–94.
[12] M.-A. Dagenais, Réhabilitation sismique des joints de chevauchement de piles de pont par chemisage en béton fibré à ultra haute performance (Seismic retrofitting of bridges piers with deficient lap splices using UHPFRC), Polytechnique Montréal, Montréal, Canada, 2014.
[13] B. Graybeal, Design and Construction of Field-cast Ultra-high Performance Concrete Connections, FHWA-HRT-14-084, U.S. Department of Transportation, Federal Highway Administration, 2014, p. 36.
[14] B. Massicotte, G. Boucher-Proulx, Seismic retrofitting of rectangular bridge piers with UHPFRC jackets, in: R. Gettu (Ed.), Proceeding of the 7th RILEM International Symposium on Fibre Reinforced Concrete: Design and Spplications - BEFIB. Chennai, India, 2008, pp. 969–975.
[15] M.A. Dagenais, B. Massicotte, Cyclic behavior of lap splices strengthened with ultra-high performance fiber reinforced concrete, ASCE J. Struct. Eng. (2016) (accepted).
[16] B. Massicotte, M.-A. Dagenais, J.-F. Garneau, Bridge pier seismic strengthening using UHPFRC, in: Proceeding of the 9th International Conference on Short and Medium Span Bridges Calgary, Canada, 2014, pp. 1–15 (paper 355).
[17] M. Kurita, T. Shioya, K. Yoshitake, H. Tanaka, B. Aarup, Properties of steel fiber-reinforced cementitious composites with 70 to 180 MPa of compressive strength, in: Proceeding of the 1st Fib Congress Osaka, Japan, 2002, pp. 1–6.
[18] C. Oesterlee, Structual Response of Reinforced UHPFRC and RC Composite Members, École Polyechnique Fédérale de Lausanne, Lausanne, 2010.
[19] T. Leutbecher, Rissbildung und Zugtragverhalten von mit Stabstahl und Fasern bewehrtem Ultrahochfesten Beton (UHPC), Kassel University, Kassel,Germany, 2007.
[20] P. Marchand, F. Baby, A. Khadour, T. Battesti, P. Rivillon, M. Quiertant, et al., Bond behaviour of reinforcing bars in UHPFRC, Mater. Struct. (2015) 1–17.
[21] M.-A. Dagenais, B. Massicotte, Tension lap splices strengthened with ultra high performance fiber reinforced concrete, ASCE J. Mater. Civil Eng. 27 (7) (2015).
[22] Y. Goto, K. Otsuka, Experimental studies on cracks formed in concrete around deformed tension bars, Tech. Rep. Tohoku Univ. 44 (1) (1979) 49–83.
[23] S. Skorobogatov, A. Edwards, The influence of the geometry of deformed steel bars on their bond strength in concrete, ICE Proc. 67 (2) (1979) 327–339.
[24] K. Jones, An Investigation of the Factors Influencing the Distribution of Splitting Stress Around Tensile Lapped Splices, Heriot-Watt University, Edinburgh, Scotland, 1993.
[25] J. Cairns, K. Jones, The splitting forces generated by bond, Mag. Concr. Res. 47 (171) (1995) 153–165.
[26] C.J. Burkhardt, Zum Tragverhalten von Übergreifungsstößen in hochfestem Beton (Behavior of lap splices in high strength concrete), RWTH Aachen University, Aachen, Germany, 2000.
[27] B.P. Richter, A New Perspective on the Tensile Strength of Lap Splices in Reinforced Concrete Members, Purdue University, West Lafayette, USA, 2012.
[28] CSA, Billet-steel Bars for Concrete Reinforcement, CAN/CSA G3018–M92 (R2007), Canadian Standards Association, Toronto, ON, Canada, 2007.
[29] ASTM, Standard Test Methods and Definitions for Mechanical Testing of Steel Products - Annex A9 Methods for Testing Steel Reinforcing Bars. A370, ASTM, West Conshohocken, PA, USA, 2010.
[30] S. Braike, Conception d'éléments préfabriqués de pont avec des bétons fibrés à haute et ultra haute performance (Design of precast deck with high and ultra high performance fibre reinforced concrete), Polytechnique Montréal, Montréal, Canada, 2007.
[31] ASTM C39, Compressive Strength of Cylindrical Concrete Specimens, C39/C39M, ASTM, West Conshohocken, PA, USA, 2010.
[32] ASTM C469, Static Modulus of Elasticity and Poison's Ratio of Concrete in Compression, C469/C469M-10, ASTM, West Conshohocken, PA, USA, 2010.
[33] A. Naaman, H. Reinhardt, Proposed classification of HPFRC composites based on their tensile response, Mater. Struct. 39 (5) (2006) 547–555.
[34] J. Houde, Study of Force-displacement Relationships for the Finite Element Analysis of Reinforced Concrete (Ph.D. Thesis), McGill University, Montreal, Quebec, 1974.
[35] Mains, Measurement of the distribution of tensile and bond stresses along reinforcing bars, ACI J. 48 (11) (1951) 225–252.
[36] W. Djabry, Contribution à l'étude de l'adhérence des fers d'armature au béton, Techn. Wiss. ETH Zürich, Zürich, 1952.
[37] D.H. Jiang, S.P. Shah, A.T. Andonian, Study of the transfer of tensile forces by bond, ACI J. 81 (24) (1984) 251–259.
[38] R.C.B. Judge, R.H. Scott, P.A.T. Gill, Strain and bond stress distributions in tension lap joints in reinforced concrete, Mag. Concr. Res. 42 (150) (1990) 5–14.
[39] R.H. Scott, Intrinsic mechanisms in reinforced concrete beam-column connection behavior, ACI Struct. J. 93 (3) (1996) 336–346.
[40] S.M. Mirza, J. Houde, Study of bond stress-slip relationships in reinforced concrete, ACI J. Proc. (1979).
[41] J.-L. Clément, Interface acier-beton et comportement des structures en beton arme: caracterisation, modelisation (Steel-concrete interface and behavior of reinforced concrete structures: characterization, modeling), Université de Paris VI, Paris, France, 1987.
[42] ACI Committee 408, in: Bond and Development of Straight Reinforcing Bars in Tension (ACI 408R-03) (Reapproved 2012), American Concrete Institute, Farmington Hills, MI, 2003, p. 49.
[43] L.A. Lutz, P. Gergely, Mechanics of bond and slip of deformed bars in concrete, ACI J. 64 (11) (1967) 711–721.
[44] F. Lagier, Étude du comportement de chevauchement d'armatures en traction directe dans du béton fibré ultra performant (Study of the behaviour of lap splices under direct tension in UHPFRC), Polytechnique Montreal, Montreal, QC, Canada, 2015.
[45] D.-Y. Yoo, J.-J. Park, S.-W. Kim, Y.-S. Yoon, Influence of reinforcing bar type on autogenous shrinkage stress and bond behavior of ultra high performance fiber reinforced concrete, Cem. Concr. Compos. 48 (2014) 150–161.
[46] J. Cairns, G.A. Plizzari, Towards a harmonised European bond test, Mater. Struct. 36 (2003) 498–506.
[47] E. Brühwiler, E. Denarié, Rehabilitation and strengthening of concrete structures using ultra-high performance fibre reinforced concrete, Struct. Eng. Int. 23 (4) (2013) 450–457.